



Probing different effects of surface MO_y and M^{n+} species ($\text{M} = \text{Cu}, \text{Ni}, \text{Co}, \text{Fe}$) for $x\text{MO}_y/\text{Ce}_{0.9}\text{M}_{0.1-x}\text{O}_{2-\delta}$ catalysts in CO oxidation

Shu-Yuan Wang^a, Na Li^a, Liang-Feng Luo^b, Wei-Xin Huang^b, Zhi-Ying Pu^c,
Yue-Juan Wang^a, Geng-Shen Hu^a, Meng-Fei Luo^{a,*}, Ji-Qing Lu^{a,*}

^a Key Laboratory of the Ministry of Education for Advanced Catalysis Materials, Institute of Physical Chemistry, Zhejiang Normal University, Jinhua 321004, China

^b Hefei National Laboratory for Physical Sciences at the Microscale and Department of Chemical Physics, University of science and Technology of China, Hefei 230026, China

^c Research Center of Analysis and Measurement, Zhejiang University of Technology, Hangzhou 310014, China



ARTICLE INFO

Article history:

Received 16 May 2013

Received in revised form 10 July 2013

Accepted 16 July 2013

Available online 24 July 2013

Keywords:

Transition metal
CO chemisorption
Solid solution
Oxygen vacancies
Synergetic effect

ABSTRACT

A series of $x\text{MO}_y/\text{Ce}_{0.9}\text{M}_{0.1-x}\text{O}_{2-\delta}$ ($\text{M} = \text{Cu}, \text{Ni}, \text{Co}, \text{Fe}$) catalysts (Ce-M) were prepared by a sol-gel method and corresponding $\text{Ce}_{0.9}\text{M}_{0.1-x}\text{O}_{2-\delta}$ catalysts (HCe-M) were obtained with an acid treatment. It was found that the Ce-M catalysts contained surface MO_y species and $\text{Ce}_{0.9}\text{M}_{0.1-x}\text{O}_{2-\delta}$ solid solution, as confirmed by the results of X-ray diffraction and Raman spectra, respectively. While the HCe-M catalysts only contained $\text{Ce}_{0.9}\text{M}_{0.1-x}\text{O}_{2-\delta}$ solid solution. CO oxidation over these catalysts revealed that the activities followed an order of Ce-Cu > Ce-Ni > Ce-Co > Ce-Fe, but were remarkably higher than the corresponding HCe-M samples. The activities of the HCe-M catalysts were closely related to their reducibility originated from the oxygen vacancies in these samples. The most active HCe-Cu catalyst had the highest content of oxygen vacancies and thus was the most reducible. For the Ce-M catalysts, the enhanced catalytic performance was due to a synergy between the surface MO_y species and the Ce-M-O solid solution, as the former provided sites for CO chemisorption and the latter promoted the activation of oxygen.

© 2013 Elsevier B.V. All rights reserved.

1. Introduction

Ceria (CeO_2) is one of the most reactive rare-earth oxides and attracted much attention due to its unique application in catalysis [1], solid oxide fuel cells [2,3], luminescence [4], UV-adsorbents [5] and semiconducting metal oxide gas sensor [6,7]. The successful applications of CeO_2 as catalytic materials are related to the facile redox cycling between trivalent and tetravalent Ce ions and the high mobility of bulk oxygen species which allows ceria to behave as an oxygen buffer [8]. It is commonly accepted that the redox property of ceria is controlled by the type, size, and distribution of oxygen vacancies as the most relevant surface defects [9]. The catalytic properties of ceria are considered to originate from the $\text{Ce}^{4+}/\text{Ce}^{3+}$ redox cycle and affected by various structural factors, such as composition modification, large surface area, and preferential exposure of reactive facets and surface defects of oxygen vacancies [10–14]. In addition, doping of ceria with different cations, such as Zr [15], Zn [16], Pr, Sn [17–19], Y, La [20], Sc, Nd, Sm, Gd, Dy, Lu [20], Pd [21] could improve the redox properties or increase the amount of oxygen vacancies and thus enhancing the

catalytic activities of ceria. Compared to pure CeO_2 , the reducibility increases with the decrease in the ionic radius of the dopant associated with the structural distortion [22]. Also, the electronic and catalytic properties of CeO_2 can be modified by metal ion substitution in CeO_2 , provided its fluorite structure is retained with higher thermal stability [23].

CO oxidation is of great practical and academic importance [24–26]. Catalytic oxidation is one of the most effective methods to remove the CO by converting CO to CO_2 [27]. Although supported noble metals (Au [28], Pt [29,30], Pd [31,32], and Ir [33]) have regarded as the most effective oxidation catalysts to eliminate CO, the high price and low availability limit their applications. Therefore, much attention has been paid to catalysts based on transition metal mixed oxides and thus become the subject of intense focus [34–36]. For example, doped-ceria with undersized lower valence ions such as Fe^{3+} have shown enhanced oxidation activity and catalytic properties through the formation of surface structural defects and a ceria-like solid solution [37,38]. Luo et al. [39] synthesized several nanosized catalysts $\text{Co}_3\text{O}_4\text{-CeO}_2$ with varying compositions and found that the catalysts, especially the ones promoted with Pd, showed markedly enhanced CO oxidation activity even at room temperature. Jung et al. [40] prepared a series of CuO-CeO_2 catalysts by a co-precipitation method and found that the best activity was obtained when the catalyst was calcined at 700 °C because a

* Corresponding authors. Tel.: +86 579 82283910; fax: +86 579 82282595.

E-mail addresses: mengfeiluo@zjnu.cn (M.-F. Luo), jiqinglu@zjnu.cn (J.-Q. Lu).

most stable Cu-Ce-O solid solution was formed on which CO could chemisorb reversibly. Luo et al. [41] studied Pd-doped mixed oxides $\text{MO}_x\text{-CeO}_2$ ($\text{M} = \text{Mn, Fe, Co, Ni, Cu}$) for CO oxidation. The results showed that a synergism effect exists between even trace amounts of exposed Pd and 3d-transition metal oxides for CO oxidation and the synergistic essential for CO oxidation should be the interaction-assisted generation of active oxygen species between Pd and MO_x .

We have previously studied the synergistic effects of PdO species on CO oxidation over PdO-CeO₂ catalysts [42]. The results showed that the activity was closely related to the catalyst structure/composition. While for the transition metals (Cu, Ni, Co, Fe) doped CeO₂ catalysts, the effect of catalyst compositions including surface MO_y ($\text{M} = \text{Cu, Ni, Co, Fe}$) species and Mⁿ⁺ cations in $\text{Ce}_{1-x}\text{M}_x\text{O}_y$ solid solutions on CO oxidation is worth further investigation.

In this work, a series of $x\text{MO}_y/\text{Ce}_{0.9}\text{M}_{0.1-x}\text{O}_{2-\delta}$ catalysts were prepared using the sol-gel method, and a comprehensive study of their catalytic performances for low-temperature oxidation of CO was conducted. After the acid treatment, surface MO_y species on the catalysts could be removed, and thus, the roles of surface MO_y species and Mⁿ⁺ cations in solid solution could be clearly distinguished. Various characterizations were performed to correlate the catalytic behaviors with the natures of the catalysts. Based on these examinations, the effects of surface MO_y species and Mⁿ⁺ cations in $\text{Ce}_{0.9}\text{M}_{0.1-x}\text{O}_{2-\delta}$ solid solution were discussed.

2. Experimental

2.1. Catalyst preparation

In the experiment, all the chemicals are of analytic grade and purchased from Sinopharm Chemical Reagent Co., Ltd., which are used without further purification.

$x\text{MO}_y/\text{Ce}_{0.9}\text{M}_{0.1-x}\text{O}_{2-\delta}$ ($\text{M} = \text{Cu, Ni, Co, Fe}$) catalysts were prepared by a citrate sol-gel method. $\text{Ce}(\text{NO}_3)_3\cdot 6\text{H}_2\text{O}$, $\text{Cu}(\text{NO}_3)_2\cdot 3\text{H}_2\text{O}$, $\text{Ni}(\text{NO}_3)_2\cdot 6\text{H}_2\text{O}$, $\text{Co}(\text{NO}_3)_2\cdot 6\text{H}_2\text{O}$, $\text{Fe}(\text{NO}_3)_3\cdot 9\text{H}_2\text{O}$ were used as the precursors, and the molar ratio of Ce and M is 9:1. Taking $x\text{CuO}/\text{Ce}_{0.9}\text{Cu}_{0.1-x}\text{O}_{2-\delta}$ catalyst as an example, $\text{Ce}(\text{NO}_3)_3\cdot 6\text{H}_2\text{O}$, $\text{Cu}(\text{NO}_3)_2\cdot 3\text{H}_2\text{O}$, and citric acid with twice moles of the metal ions were dissolved in deionized (DI) water. The mixture was heated at 90 °C under stirring until it became a viscous gel and then dried overnight at 120 °C. The resulting solid was calcined at 800 °C for 4 h with a heating rate of 10 °C min⁻¹ to obtain the final material $x\text{CuO}/\text{Ce}_{0.9}\text{Cu}_{0.1-x}\text{O}_{2-\delta}$. Catalysts with other dopants were prepared in a similar manner. The catalysts were denoted as Ce-Cu, Ce-Ni, Ce-Co and Ce-Fe.

The obtained Ce-Ni, Ce-Cu catalysts were subjected to nitric acid treatment for comparison. Taking Ce-Cu catalyst as an example, the catalyst was immersed and stirred in concentrated nitric acid (HNO_3 , 30 ml, 15.2 mol/L) at 100 °C for 4 h then filtered. The above process was repeated for three times. Finally, the obtained solid was washed with plenty of deionized water to remove the residual nitric acid and dried at 90 °C. The Ce-Co, Ce-Fe catalysts were treated by hydrochloric acid (HCl, 30 ml, 12.4 mol/L) in a similar manner as the Ce-Ni, Ce-Cu catalysts. The treated Ce-Co, Ce-Fe catalysts were washed thoroughly with deionized water until these samples were free of Cl⁻, as evidenced with an aqueous solution of AgNO_3 (0.1 mol/L). The catalysts were denoted as HCe-Cu, HCe-Ni, HCe-Co and HCe-Fe.

Supported CuO/HCe-M ($\text{M} = \text{Cu, Ni, Co, Fe}$) and CuO/CeO₂ catalysts with a CuO loading of 5 wt.% were prepared using a conventional impregnating method. In a typical process, 0.24 g $\text{Cu}(\text{NO}_3)_2\cdot 3\text{H}_2\text{O}$ was dissolved in deionized water (1 ml), and then 1.5 g of the support was immersed in the solution for 12 h. The mixture was heated at 90 °C and then dried overnight at 120 °C. The

resulting solid was calcined at 300 °C for 4 h in air to yield the final catalysts. The catalysts were denoted as CuO/HCe-Cu, CuO/HCe-Ni, CuO/HCe-Co, CuO/HCe-Fe and CuO/CeO₂. Pure CeO₂ powder was obtained by direct thermal decomposition of $\text{Ce}(\text{NO}_3)_3\cdot 6\text{H}_2\text{O}$ at 800 °C for 4 h.

2.2. Characterizations

X-ray diffraction (XRD) patterns were collected on a PANalytical X'Pert PRO MPD powder diffractometer using Cu K α radiation ($\lambda = 0.15418 \text{ nm}$). The working voltage was 40 kV and the working current was 40 mA. The patterns were collected in a 2 θ range from 10 to 90°. The mean crystallite size were determined from line-broadening measurements on the (111) peak of CeO₂, using the Scherrer equation: $D = K\lambda/\beta \cos \theta$, where λ is the synchrotron wavelength ($\lambda = 0.154178 \text{ nm}$), K is the particle shape factor, taken as 0.94 for spherical particles, β is the full-width at half maximum height (FWHM) in radians. The β -values were carefully determined by a least-square fit of a Gaussian function. The lattice parameter was determined by the Rietveld method using JADE 6.5 software.

Elemental compositions of the catalysts were determined by X-ray fluorescence (XRF) analysis, on an ARL ADVANT'X Intelli Power 4200 scanning X-ray fluorescence spectrometer. The results were analyzed using UniQuant non-standard sample quantitative analysis software.

Raman spectra were recorded on a Renishaw RM1000 with a confocal microprobe Raman system using an excitation laser line of 325 nm, in a range from 350 to 1000 cm⁻¹.

Reducibility of the catalysts was measured by the hydrogen temperature-programmed reduction (H₂-TPR) technique. 50 mg of the sample was placed in a quartz reactor connected to a homemade TPR apparatus and the reactor was heated from 40 to 800 °C with a heating rate of 10 °C min⁻¹, in a reducing atmosphere of mixed H₂ (5 vol.%) and N₂ (95 vol.%) with a total flow rate of 30 ml min⁻¹. The amount of H₂ uptake during the reduction was measured by a thermal conductivity detector (TCD), calibrated by using a known amount of pure CuO powder. The water produced in TPR was trapped on a 5 Å molecular sieve.

Diffuse reflectance infrared Fourier transform (DRIFT) spectra of the samples were recorded using a Nicolet 6700 spectrometer equipped with a mercury-cadmium-tellurium (MCT) detector and a diffuse reflectance cell (Harrick CHC-CHA-3), with a resolution of 4 cm⁻¹. An accumulation of 64 scans was used for collecting the spectra. About 20 mg of the catalyst was placed in the cell and pretreated at 300 °C for 1 h in a flow of Ar (30 ml min⁻¹) in order to remove water and carbonate in the catalyst. Subsequently, the system was cooled down to 30 °C and the background spectrum was recorded. After the introduction of the gas mixture (1 vol.% CO in Ar, 30 ml min⁻¹) for 30 min, the catalyst was purged with Ar for 30 min to remove the gaseous and physisorbed CO, and then a spectrum was collected.

2.3. Catalytic testing

CO oxidation experiments were conducted in a packed bed quartz tube (i.d. = 6 mm and length = 35 cm) operated isothermally at atmospheric pressure, in the temperature range of 80–500 °C. 200 mg of the catalyst was loaded into the reactor and the reaction temperature was monitored by a thermocouple placed at the center of the catalyst bed. A mixture of 1 vol.% CO and 1 vol.% O₂ balanced with N₂ was introduced as the reactants. The total flow rate was 40 ml min⁻¹ and the space velocity was 12,000 ml g⁻¹ h⁻¹. The catalyst was directly exposed to the reaction without any pretreatment. The CO concentration in the reactor effluent was analyzed using an Agilent 6850 gas chromatograph equipped with a thermal conductivity detector (TCD) and an HP PLOT (30 m × 0.32 mm × 12 μm)

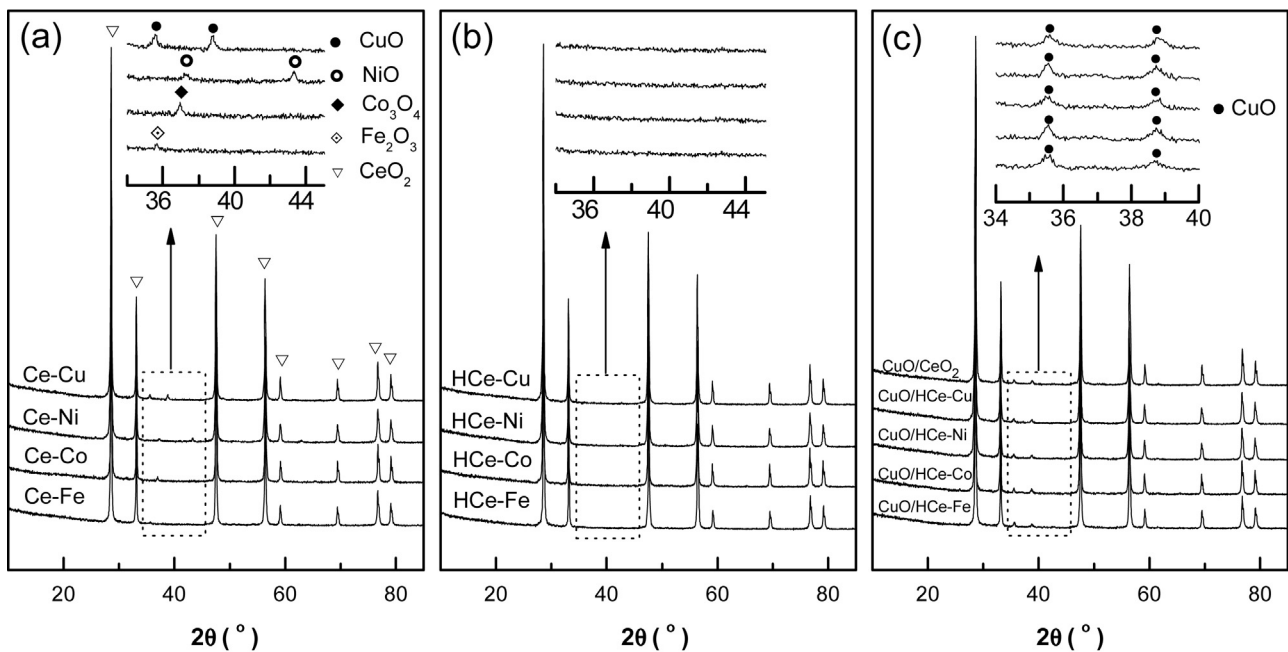


Fig. 1. XRD patterns of (a) Ce-M, (b) HCe-M and (c) CuO/HCe-M ($M = \text{Cu}, \text{Co}, \text{Ni}, \text{Fe}$) and CuO/CeO₂ catalysts.

column. The activities of the catalysts were then evaluated on the basis of CO conversion, which can be calculated with the CO concentrations in the reactant gas and in the effluent gas. The equation is as follows:

$$\text{CO conversion} (\%) = \frac{[\text{CO}]_{\text{in}} - [\text{CO}]_{\text{out}}}{[\text{CO}]_{\text{in}}} \times 100 \quad (1)$$

where $[\text{CO}]_{\text{in}}$ is the CO concentrations in the feed stream, and $[\text{CO}]_{\text{out}}$ is the CO concentrations in the effluent gases.

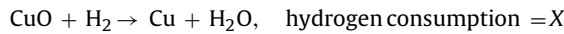
Reaction rate of the prepared catalysts based on per unit catalyst was calculated as follows:

$$r_{\text{CO}} = \frac{F_{\text{CO}} \times X_{\text{CO}}}{W_{\text{Cat}}} \quad (2)$$

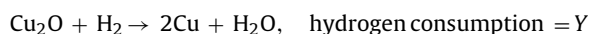
where F_{CO} is the CO molar gas flow rate in mol s^{-1} , X_{CO} is the conversion of CO, W_{Cat} is the catalyst weight in grams, and r_{CO} is the reaction rate in $\text{mol}_{\text{CO}} \text{ g}_{\text{cat}}^{-1} \text{ s}^{-1}$.

The dispersion of Cu on the surface of catalysts was measured by N₂O chemical adsorption experiments reported by Van Der Grift et al. [43]. 0.05 mg CuO/HCe-M catalyst was first loaded in quartz tube and pretreated at 200 °C for 1 h under Ar flow (30 ml min⁻¹). After sample was cooled to 50 °C, reduction agent (5% H₂/N₂ mixture, 30 ml min⁻¹) was shifted; sample was heated to 500 °C at a rate of 10 °C min⁻¹. The consumption of hydrogen was analyzed by thermal conductivity detector (TCD). The amount of hydrogen consumption in first TPR was denoted as X. And then, the catalyst bed was purged with Ar and cooled to 50 °C. Surface copper atoms were oxidized in a N₂O at 50 °C for 0.5 h. Finally, samples were flushed with Ar to remove the oxidant and cooled to 50 °C to start another TPR run. Hydrogen consumption in the second TPR was denoted as Y. The calculation of the dispersion of Cu is followed:

All copper atoms were reduced in the first TPR:



Surface copper atoms that were oxidized to Cu₂O by N₂O at 50 °C were reduced in the second TPR:



And the dispersion of Cu and exposed Cu surface area were calculated as:

$$D = \left(2 \times \frac{Y}{X} \right) \times 100\% \quad (3)$$

TOF (turnover frequency) of catalysts based on the dispersion of CuO was calculated as follows:

$$\text{TOF} = \frac{F_{\text{CO}} \times X_{\text{CO}}}{n_{\text{CuO}} \times D} \quad (4)$$

where F_{CO} is the CO molar gas flow rate in mol s^{-1} , X_{CO} is the conversion of CO at 100 °C, n_{CuO} is the weight loading of CuO in the catalyst, and D is the dispersion of CuO.

3. Results

3.1. Structural characterization

Fig. 1 shows the XRD patterns of the Ce-M, HCe-M and CuO/HCe-M ($M = \text{Cu}, \text{Co}, \text{Ni}, \text{Fe}$) and CuO/CeO₂ catalysts. Characteristic peak of cubic CeO₂ phase are observed in all the catalysts. In addition, weak peaks characteristic of Fe₂O₃ phase at 35.7°, Co₃O₄ phase at 37.0°, NiO phase at 37.3 and 43.1°, CuO phase at 35.5 and 38.8° are detected (**Fig. 1a** inset). This indicates that corresponding metal oxides (MO_y) are formed on the surface of Ce-M catalysts. However, the XRD patterns of the HCe-M catalysts reveal the absence of MO_y species as shown in **Fig. 1b** (inlet), indicating that the surface MO_y species have been removed on the surface of Ce-M catalysts after the acid treatment or these species are beyond the detection limit of XRD technique, which can not detect crystallite sizes below 3 nm. In the case of CuO/HCe-M and CuO/CeO₂ catalysts (**Fig. 1c**), two weak diffraction peaks due to CuO phase are detected, and it also can be found that the support (HCe-M) hardly affects the intensities of the CuO peaks.

Table 1 shows the lattice parameters, crystallite size, and the contents of MO_y and Mⁿ⁺ in the catalysts. The lattice parameters of all the catalysts decrease slightly compared to that of pure CeO₂ (JCPDS: 34-0394), indicating that some Mⁿ⁺ cations incorporate into the ceria lattice to form the Ce_{0.9}M_{0.1-x}O_{2-δ} solid solution. This is because the radius of Cu²⁺ (0.72 Å), Ni²⁺ (0.72 Å), Co²⁺

Table 1

Cell parameters, crystallite size of CeO_2 , surface MO_y and M^{n+} contents of Ce-M, HCe-M, CuO/HCe-M and CuO/ CeO_2 catalysts.

Catalyst	Cell parameter (nm) ^a	Crystallite size (nm)	Content (wt.%) ^b	
			Surface MO_x	M^{n+}
Ce-Fe	0.5410(1)	39.4	3.37	0.24
Ce-Co	0.5408(0)	42.1	3.48	0.26
Ce-Ni	0.5409(2)	34.8	3.63	0.32
Ce-Cu	0.5408(7)	40.2	4.20	0.30
HCe-Fe	0.5409(6)	38.8	—	0.24
HCe-Co	0.5408(9)	42.2	—	0.26
HCe-Ni	0.5410(0)	36.4	—	0.32
HCe-Cu	0.5409(8)	41.6	—	0.30
CuO/HCe-Fe	0.5409(8)	38.1	4.96	—
CuO/HCe-Co	0.5409(1)	42.3	4.92	—
CuO/HCe-Ni	0.5409(7)	35.9	4.93	—
CuO/HCe-Cu	0.5410(5)	39.4	4.98	—
CuO/ CeO_2	0.5412(0)	43.0	4.95	—

^a Lattice parameters were calculated from characteristic XRD peaks of CeO_2 planes using the MDI Jade Program.

^b Determined by XRF technique.

(0.74 \AA)/ Co^{3+} (0.63 \AA) or Fe^{3+} (0.64 \AA) is smaller than that of Ce^{4+} (0.97 \AA), leading to a decline in lattice parameter when Ce^{4+} are partially substituted by M^{n+} cations to form a $\text{Ce}_{0.9}\text{M}_{0.1-x}\text{O}_{2-\delta}$ solid solution. Furthermore, the formation of $\text{Ce}_{0.9}\text{M}_{0.1-x}\text{O}_{2-\delta}$ solid solution inhibits the growths of crystallite size, as the crystallite sizes of CeO_2 in Ce-M, HCe-M and CuO/HCe-M catalysts are from 35.8 nm to 42.3 nm , which is slightly smaller than that of CeO_2 (43.0 nm) in CuO/ CeO_2 catalyst. Comparison of the metal contents before and after the acid treatment, it is found that the metal loadings in the acid-treated samples are much lower than those in the corresponding as-prepared samples, indicating the acid treatment removed most of the surface MO_y species. A quantitative calculation of the HCe-M samples reveals that the substitution ratio of M in the CeO_2 matrix is about 0.74%, 0.76%, 0.93%, and 0.81% for the HCe-Fe, HCe-Co, HCe-Ni and HCe-Cu samples, respectively (see Table S1, Supporting Information).

It should be clarified that the supported CuO/HCe-M and CuO/ CeO_2 catalysts contain only surface CuO species, without Cu^{2+} ions in the ceria lattice. To prove this, the CuO/HCe-M and

CuO/ CeO_2 catalysts were treated by nitric acid, and the XRF technique was taken to analyze the contents of CuO in the remaining solid (see Table S2, Supporting Information). It can be seen that no Cu element was found for the CuO/HCe-Fe, CuO/HCe-Co, CuO/HCe-Ni, and CuO/ CeO_2 catalysts after the nitric acid treatment. While for the CuO/HCe-Cu catalyst (after the nitric acid treatment), the content of Cu element was same (0.3%) as that in the HCe-Cu supporter.

Fig. 2 shows the Raman spectra of the catalysts with 325 nm excitation laser line. All the catalysts have a strong band at 463 cm^{-1} and two weak bands at 540 and 588 cm^{-1} . The band at 463 cm^{-1} could be ascribed to the F_{2g} vibration mode of fluorite structure of CeO_2 [44,45]. The band around 540 cm^{-1} could be attributed to the defect space which includes an O^{2-} vacancy [12] and the band at 588 cm^{-1} could be ascribed to the vacancy-interstitial (Frenkel-type) oxygen defects in ceria [46]. The peak areas of the bands at 463 , 540 and 588 cm^{-1} were calculated based on Raman spectra (**Fig. 2**), which were denoted as A_2 and A_1 , respectively. The ratio of A_1/A_2 reflects the concentration of oxygen vacancies in the catalysts [47]. It is clear that A_1/A_2 values of the Ce-M, HCe-M catalysts are higher than that of CeO_2 (0.70). This may be due to the fact that M^{n+} cations penetrated into the ceria lattice, resulting in a larger amount of oxygen vacancies created in these samples. This also suggests that the formation of $\text{Ce}_{0.9}\text{M}_{0.1-x}\text{O}_{2-\delta}$ solid solution, which is in good agreement with the XRD results (**Fig. 1**).

In order to determine the mobility of oxygen species in different samples, H_2 -TPR experiments of the Ce-M, HCe-M and CeO_2 catalysts were conducted, and the results are shown in **Fig. 3**. For the Ce-M catalyst (**Fig. 3a**), peaks at $195\text{ }^\circ\text{C}$ (for Ce-Cu), $291\text{ }^\circ\text{C}$ (for Ce-Ni), $365\text{ }^\circ\text{C}$ (for Ce-Co), and $438\text{ }^\circ\text{C}$ (for Ce-Fe) could be assigned to the reduction of highly dispersed or small crystallite transition metal oxides CuO , NiO , Co_3O_4 , and Fe_2O_3 on the surface of catalysts, respectively. The peaks at 249 and $287\text{ }^\circ\text{C}$ for Ce-Cu catalyst, the peaks at 382 and $424\text{ }^\circ\text{C}$ for Ce-Ni catalyst could be assigned to the reduction of the transition metal oxides (CuO and NiO) that weakly and strongly interacted with CeO_2 [48,49]. As for the Ce-Co and Ce-Fe catalysts, the peaks at 420 and $464\text{ }^\circ\text{C}$ (Ce-Co), 598 and $717\text{ }^\circ\text{C}$ (Ce-Fe) are related to the stepwise reduction of the transition metal oxides, involving in CoO and Fe_3O_4 intermediates [50,51]. Among these samples, the Ce-Cu catalyst is the most reducible, while the Ce-Fe catalyst is the least reducible. For the acid-treated catalysts,

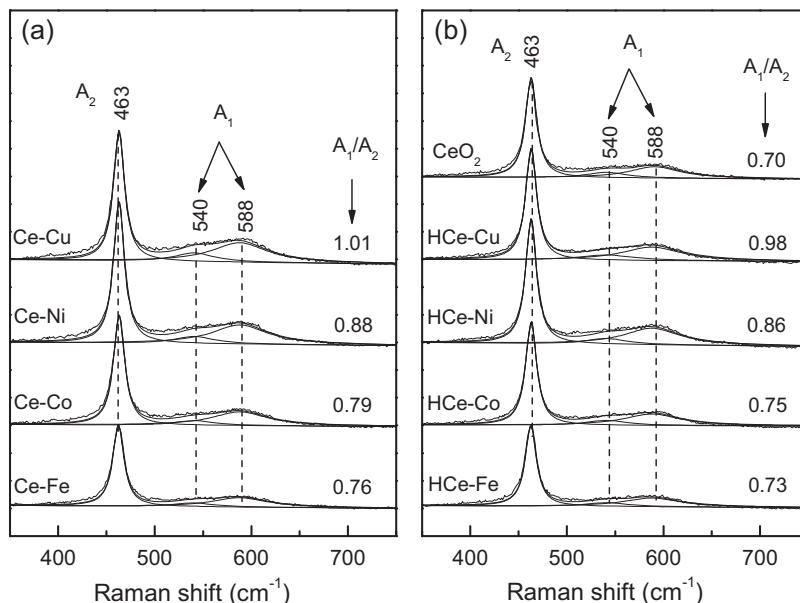


Fig. 2. Raman spectra ($\lambda_{\text{ex}} = 325\text{ nm}$) of (a) Ce-M, (b) HCe-M and CeO_2 catalysts.

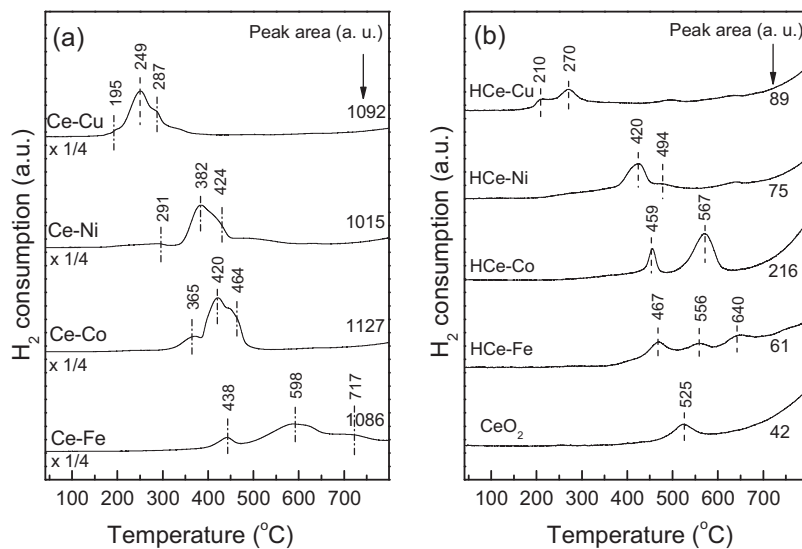


Fig. 3. H₂-TPR profiles of (a) Ce-M and (b) HCe-M and CeO₂ catalysts.

the reduction peaks shift to a higher temperature as can be seen in Fig. 3b, suggesting that the reducibility of the HCe-M catalysts is somehow inhibited. For the pure CeO₂ the only peak at 525 could be assigned to the reduction of surface oxygen [52]. Peaks at 210 and 270 °C for HCe-Cu catalyst, 420 and 494 °C for HCe-Ni catalyst, 459 and 567 °C for HCe-Co catalyst, 467, 556 and 640 °C for HCe-Fe catalyst could be assigned to the reduction of Mⁿ⁺ cations in the subsurface and in the CeO₂ lattice, respectively. Comparison of the reduction peak positions of the HCe-M clearly reveal different reducibility of these samples, which follows the same trend as the Ce-M samples, namely, the HCe-Cu is the most reducible while the HCe-Fe and pure CeO₂ are the least reducible. The integrated areas of the TPR peaks for the catalysts were also calculated and listed in Fig. 3. Obviously, the reduction peak areas of the HCe-M catalysts are much lower compared to the corresponding Ce-M catalysts, probably due to the fact that the surface MO_y species were removed by the acid treatment.

3.2. DRIFT spectra of CO chemisorption on the catalysts

Fig. 4 shows the DRIFT spectra of CO chemisorption over the Ce-M and CuO/HCe-M catalysts. It can be seen that there are two peaks in regions of 1200–1700 and 1800–2250 cm⁻¹. The former peaks at 1200–1700 cm⁻¹ is characteristic of carbonate or carboxylate adsorbed on the catalyst surface [53,54], and the latter adsorption peak of 2115 cm⁻¹ is attributed to chemisorbed CO over Cu⁺ cations [55]. However, IR bands corresponding to CO adsorbed on the Ce-Ni (Ni²⁺-CO; 2220, 2212 cm⁻¹ [56]), Ce-Co (Co²⁺-CO; 2207, 2217 cm⁻¹ [57,58]), Ce-Fe (Fe²⁺-CO; 2150, 2180 cm⁻¹ [59], Fe³⁺-CO; 2175 cm⁻¹ [60,61]) catalysts were not obvious. Also, for the HCe-M samples, no obvious CO chemisorption is observed (Fig. S2, Supporting Information). Moreover, the higher intensities of the bands for the CuO/HCe-M and CuO/CeO₂ catalysts than that of the Ce-Cu catalyst could be attributed to a higher amount of CuO species on the surface of the former catalysts (Table 1).

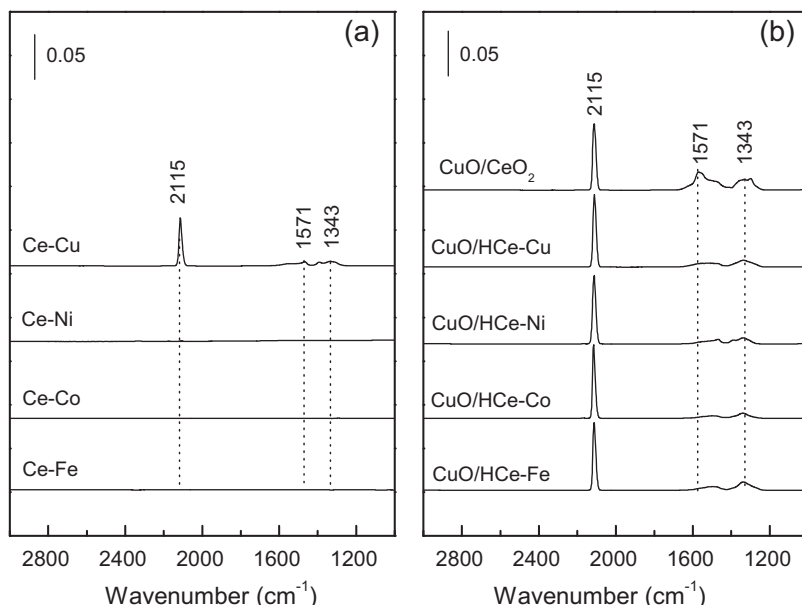


Fig. 4. In situ DRIFT spectra for CO chemisorption on (a) Ce-M and (b) CuO/HCe-M, CuO/CeO₂ catalysts.

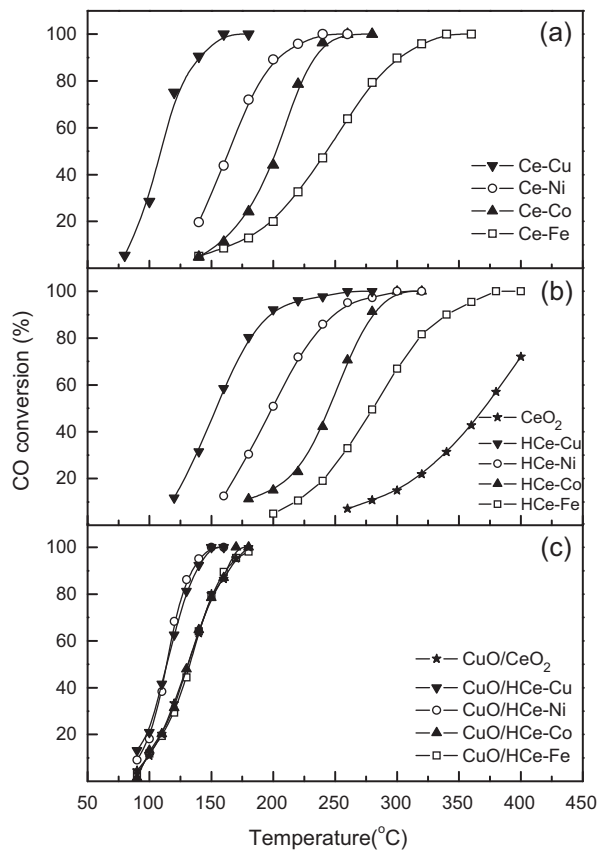


Fig. 5. CO oxidation over (a) Ce-M, (b) HCe-M, CeO₂ and (c) CuO/HCe-M, CuO/CeO₂ catalysts.

3.3. Catalytic activity

The activities of the Ce-M, HCe-M, CeO₂, CuO/HCe-M and CuO/CeO₂ catalysts are given in Fig. 5. It can be seen from Fig. 5a that for the Ce-M catalysts, the activity follows the trend of Ce-Cu > Ce-Ni > Ce-Co > Ce-Fe, with the Ce-Cu catalyst possessing the highest activity with a T_{50} (temperature at which CO conversion is 50%) of 108 °C. However, after the acid treatment (Fig. 5b), the activities of the HCe-M catalysts are much lower than the corresponding Ce-M catalysts, but they still follow the same trend as the Ce-M catalysts. Moreover, the HCe-M catalysts are much more active compared to the pure CeO₂. The HCe-Cu catalyst has the highest activity among these catalysts with a T_{50} of 154 °C, which is about 50 °C higher than that of the Ce-Cu catalyst. Interestingly, when CuO is supported on the HCu-M supports, the activities become essentially the same (Fig. 5c), with the CuO/HCe-Cu, CuO/HCe-Ni possessing slightly higher activities than the CuO/HCe-Fe, CuO/HCe-Co and CuO/CeO₂. For a better understanding of the catalytic activity of CuO/HCe-M catalysts, turnover frequencies (TOFs) based on the dispersion of CuO species in the catalysts are calculated and listed in Table 2. It can be seen that the TOFs values hardly change, varying from 1.3 to $1.8 \times 10^{-3} \text{ s}^{-1}$.

4. Discussion

4.1. Structural properties of Ce-M, HCe-M, CuO/HCe-M and CuO/CeO₂ catalysts

In this work, CeO₂-based catalysts were prepared using different methods, namely, the Ce-M (M = Cu, Ni, Co, Fe) catalysts were prepared by a sol-gel method and the CuO/HCe-M, CuO/CeO₂ catalysts

Table 2

Relevant parameter for calculating the TOFs of CuO/HCe-M (M = Cu, Ni, Co, Fe) and CuO/CeO₂ catalysts.

Catalyst	X_{CO}^{a}	Dispersion ^b	Particle size of CuO (nm) ^c	TOF ($\times 10^{-3} \text{ s}^{-1}$)
CuO/HCe-Fe	0.12	0.21	4.8	1.4
CuO/HCe-Co	0.10	0.19	5.3	1.3
CuO/HCe-Ni	0.18	0.28	3.6	1.6
CuO/HCe-Cu	0.21	0.29	3.4	1.8
CuO/CeO ₂	0.13	0.22	4.5	1.4

^a Conversion of CO at 100 °C.

^b Dispersion of CuO calculated based on the N₂O chemical adsorption.

^c Assuming that $d_{\text{CuO}} (\text{nm}) = 1/D$ (dispersion).

were prepared by a conventional impregnation method. Various techniques are employed in order to obtain structural and surface information of the catalysts. The results show that the Ce-M catalysts calcined at 800 °C mainly contain surface MO_y species and Mⁿ⁺ cations in form of Ce_{0.9}M_{0.1-x}O_{2-δ} solid solution. The surface MO_y species are evidenced by the XRD (Fig. 1a) and H₂-TPR (Fig. 3a) results, while the formation of Ce_{0.9}M_{0.1-x}O_{2-δ} solid solution is confirmed by Raman spectroscopy (Fig. 2a) and cell parameters of catalysts derived from XRD results (Table 1). After the acid treatment, the surface MO_y species could be removed and the remaining Ce_{0.9}M_{0.1-x}O_{2-δ} solid solution keeps their structures, which are confirmed by XRD (Fig. 1b) and Raman spectroscopy (Fig. 2b). In addition, the surface MO_y species and Mⁿ⁺ cations in the Ce_{0.9}M_{0.1-x}O_{2-δ} solid solution are quantitatively evaluated by XRF technique (Table 1), and the results reveal that the content of Mⁿ⁺ cations is much lower than that on the surface of catalysts. By this set of design, the MO_y species and Mⁿ⁺ cations were effectively distinguished, and their contributions in CO oxidation were discussed.

4.2. Roles of surface MO_y species and oxygen vacancy in CO oxidation

For CO oxidation over supported metal catalysts, the activity is mainly influenced by activation of CO and oxygen. Chemisorption and activation of CO molecules usually take place on the surface of metal/metal oxide species, and it has been generally recognized that the chemisorption of CO is important for the catalysts in CO oxidation, as the activation barrier of CO molecules could be significantly lowered. The activation of oxygen is usually related to the reducibility of the support, especially when reducible oxides such as CeO₂ are used as the support. Due to the presence of oxygen vacancies, CeO₂-based solid solution could serve as an oxygen supplier in the formation of superoxide species (O₂⁻) by gas-phase oxygen reacting with oxygen vacancies on its surface or promote lattice oxygen migration and direct involvement in CO oxidation [62,63]. Thus, the formation of oxygen vacancies in the sample is helpful to the activation of oxygen species on the catalyst surface. For example, Teschner et al. [64] studied the Pt/CeO₂ catalyst in CO oxidation and found that the oxygen vacancies in the CeO₂ was beneficial for the activation of gas oxygen, and thus lowered apparent activation energy of CO oxidation.

For the HCe-M samples, the chemisorption of CO is very limited, as evidenced by the DRIFT results (see Fig. S2, Supporting Information). This could be correlated to the removal of surface MO_y species by the acid treatment. Then, the catalytic performance of these HCe-M samples strongly depends on their reducibility which is related to the content of oxygen vacancies in the samples. The H₂-TPR results (Fig. 3b) clearly show that the reducibility of the HCe-M samples follows the order of HCe-Cu > HCe-Ni > HCe-Co > HCe-Fe, which is most likely related to the amount of oxygen vacancies in these samples, as the Raman spectroscopic results (Fig. 2) indicated that the

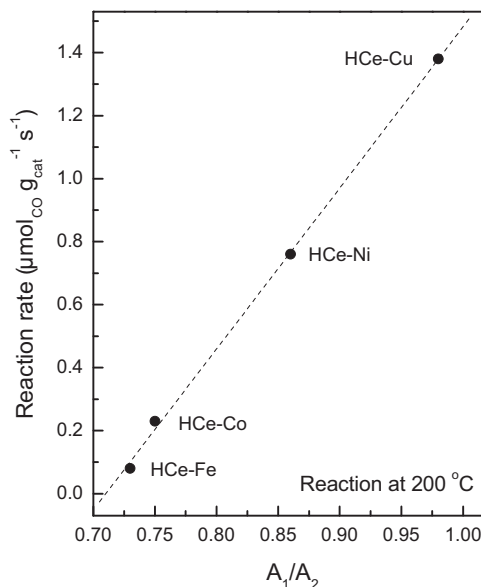


Fig. 6. Correlation between A_1/A_2 value and reaction rates for HCe-M catalysts.

relative concentration of oxygen vacancies in these samples follow the same trend of the reducibility.

The effects of reducibility of the HCe-M materials on the catalytic activity could be confirmed by the correlation between the relative concentration of oxygen vacancies and specific reaction rates on these samples, as shown in Fig. 6. It is clearly seen that the reaction rates are significantly enhanced with increasing concentration of oxygen vacancies (A_1/A_2) in the samples. For example, the HCe-Cu catalyst has the highest activity ($1.38 \mu\text{mol CO g}_{\text{cat}}^{-1} \text{s}^{-1}$), HCe-Ni and HCe-Co catalysts have the medium activity (0.76 and $0.23 \mu\text{mol CO g}_{\text{cat}}^{-1} \text{s}^{-1}$, respectively), while the HCe-Fe catalyst has the lowest activity ($0.08 \mu\text{mol CO g}_{\text{cat}}^{-1} \text{s}^{-1}$). These results strongly confirm the role of oxygen vacancies (by doping M cations into the CeO₂ matrix) in CO oxidation, which are consistent with our previous findings [42,47,65] that the introduction of Pd, Pr and Tb ions into the CeO₂ lattice could effectively enhance the formation of oxygen vacancies, and consequently accelerates the activity of CO oxidation.

Concerning the Ce-M catalysts, situation becomes complicated because of the presence of surface MO_y species on these samples. Since the activities of the Ce-M catalysts are higher than those of the corresponding HCe-M catalysts, it reveals the important role of surface MO_y species in the reaction, most likely resulting from the chemisorption and activation of CO molecules on these surface species. In the present work, it could be observed from Fig. 4a that only for the Ce-Cu catalyst, the band at 2115 cm^{-1} corresponding to Cu⁺ carbonyl (Cu⁺-CO) is observed at low temperature (50 °C). In contrast, no obvious CO chemisorption bands are observed on the Ce-Ni, Ce-Co and Ce-Fe catalysts, suggesting that the M' (M' = Ni²⁺, Co²⁺/Co³⁺, Fe²⁺/Fe³⁺) cations are difficult to adsorb CO molecules in the current conditions. A possible explanation of this phenomenon is the lower thermal stability of the M'-CO species under the DRIFTS conditions or strong bonding of surface oxygen anion with M' species. For example, Ozkan et al. [66] reported that the weakly bands associated with adsorbed CO over a 2% CoO_x/CeO₂ catalyst decreased with elevated temperature and CO chemisorption on supported Ni catalyst was sensitive to parameters such as CO pressure and adsorption temperature [67]. While for Fe supported catalysts, adsorption of CO molecules was greatly influenced by the different treatment conditions [59,60]. Nevertheless, although no obvious CO chemisorption was observed on the Ce-M catalysts (except the

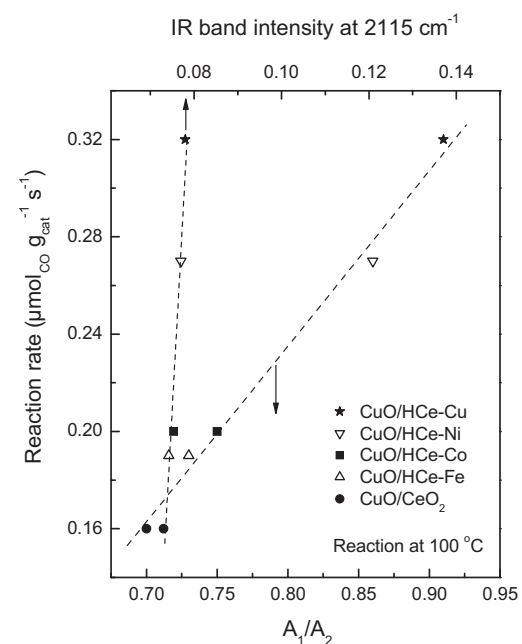


Fig. 7. Correlation of IR band intensity at 2115 cm^{-1} , A_1/A_2 value and reaction rates of CuO/HCe-M and CuO/CeO₂ catalysts.

Ce-Cu catalyst), the roles of surface MO_y species are significant, which is evidenced by the fact that the Ce-M catalysts are much more active than the acid-treated HCe-M catalysts (Fig. 5a and b).

Therefore, the catalytic performance of the Ce-M catalyst depends on the synergy of surface MO_y species and the Mⁿ⁺ cations in the form of Ce-M-O solid solution, as the surface MO_y species provide sites for CO chemisorption and the Ce-M-O solid solution facilitates the activation of oxygen species (enhanced reducibility). Similar findings have been also reported in our previous work [68]. The highest activity was obtained on the Ce-Cu catalyst, due to the fact that it has the most pronounced ability of CO chemisorption (Fig. 4a) and reducibility (Fig. 3a), while the Ce-Fe has the lowest activity because of its limited ability of CO chemisorption and reducibility.

The synergy of surface MO_y species and Ce-M-O solid solution is again confirmed by the catalytic behaviors of the CuO/HCe-M and CuO/CeO₂ catalysts. The CuO/HCe-M catalysts are more active than the HCe-M samples (Fig. 5), suggesting the role of surface CuO species in the reaction for providing sites for CO chemisorption. Moreover, Fig. 7 presents the correlation of IR band intensity at 2115 cm^{-1} , reaction rates, and A_1/A_2 value for CuO/HCe-M and CuO/CeO₂ catalysts based on the data in Figs. 3 and 4. It is found that the reaction rates increase with the A_1/A_2 values but are essentially independent of the IR band intensity. Such a correlation also implies that the effects of support reducibility on the reactivity might be more pronounced than that of the surface MO_y species.

5. Conclusion

This work demonstrates the relationship between the structural property and catalytic behavior of CO oxidation over Ce-M, HCe-M, CuO/HCe-M catalysts. The Ce-M catalysts contain surface MO_y species and Ce-M-O solid solution, while the HCe-M samples contain only Ce-M-O solid solution. The HCe-M samples have enhanced reducibility due to the formation of oxygen vacancies by the doping of M cations in the CeO₂ lattice, which consequently promotes the activity. The enhanced activity of the Ce-M compared to that of the HCe-M lies in the synergy of the surface MO_y species and the solid

solution, with the former providing sites for CO chemisorption and the latter for oxygen activation. Moreover, the support reducibility seems exert more influence on the activity than the surface MO_y species.

Acknowledgements

This work is financially supported by Natural Science Foundation of China (Grant Nos. 21173195 and 21203167) and the Program for Changjiang Scholars and Innovative Research Team in Chinese Universities (IRT0980).

Appendix A. Supplementary data

Supplementary data associated with this article can be found, in the online version, at <http://dx.doi.org/10.1016/j.apcatb.2013.07.037>.

References

- [1] P.X. Huang, F. Wu, B.L. Zhu, X.P. Gao, H.Y. Zhu, T.Y. Yan, W.P. Huang, S.H. Wu, D.Y. Song, *J. Phys. Chem. B* 109 (2005) 19169–19174.
- [2] B.C.H. Steele, A. Heinzel, *Nature* 414 (2001) 345–352.
- [3] C.W. Sun, Z. Xie, C.R. Xia, H. Li, L.Q. Chen, *Electrochim. Commun.* 8 (2006) 833–838.
- [4] X.J. Yu, P.B. Xie, Q.D. Su, *Phys. Chem. Chem. Phys.* 3 (2001) 5266–5269.
- [5] L.W. Qian, J. Zhu, W.M. Du, X.F. Qian, *Mater. Chem. Phys.* 115 (2009) 835–840.
- [6] D. Barreca, E. Comini, A. Gasparotto, C. Maccato, C. Maragno, G. Sberveglieri, E. Tondello, *J. Nanosci. Nanotechnol.* 8 (2008) 1012–1016.
- [7] N. Izu, W. Shin, N. Murayama, S. Kanzaki, *Sens. Actuators B: Chem.* 87 (2002) 95–98.
- [8] Y.H. Tang, H. Zhang, L.X. Cui, C.Y. Ouyang, S.Q. Shi, W.H. Tang, H. Li, J.S. Lee, L.Q. Chen, *Phys. Rev. B* 82 (2010) 125104.
- [9] F. Esch, S. Fabris, L. Zhou, T. Montini, C. Africh, P. Fornasiero, G. Comelli, R. Rosei, *Science* 309 (2005) 752–755.
- [10] M. Sanchez-Dominguez, L.F. Liotta, G. Di Carlo, G. Pantaleo, A.M. Venezia, C. Solans, M. Boutonnet, *Catal. Today* 158 (2010) 35–43.
- [11] L. Qi, C.G. Tang, L. Zhang, X.J. Yao, Y. Cao, L.C. Liu, F. Gao, L. Dong, Y. Chen, *Appl. Catal. B* 127 (2012) 234–245.
- [12] Z.L. Wu, M.J. Li, J. Howe, H.M. Meyer, S.H. Overbury, *Langmuir* 26 (2010) 16595–16606.
- [13] M.F. Luo, Y.P. Song, J.Q. Lu, X.Y. Wang, Z.Y. Pu, *J. Phys. Chem. C* 111 (2007) 12686–12692.
- [14] L. Meng, J.J. Lin, Z.Y. Pu, L.F. Luo, A.P. Jia, W.X. Huang, M.F. Luo, J.Q. Lu, *Appl. Catal. B* 119–120 (2012) 117–122.
- [15] A. Martínez-Arias, M. Fernández-García, A.B. Hungri'a, A. Iglesias-Juez, O. Gálvez, J.A. Anderson, J.C. Conesa, J. Soria, G. Munuera, *J. Catal.* 214 (2003) 261–272.
- [16] O.H. Laguna, M.A. Centeno, F. Romero-Sarria, J.A. Odriozola, *Catal. Today* 172 (2011) 118–123.
- [17] T.Y. Zhang, S.P. Wang, Y. Yu, Y. Su, X.Z. Guo, S.R. Wang, S.M. Zhang, S.H. Wu, *Catal. Commun.* 9 (2008) 1259–1264.
- [18] Z.X. Song, W. Liu, H. Nishiguchi, A. Takami, K. Nagaoka, Y. Takita, *Appl. Catal. A* 329 (2007) 86–92.
- [19] B.M. Reddy, P. Bharali, P. Saikia, A. Khan, S. Loridan, M. Muhler, W. Grünert, *J. Phys. Chem. C* 111 (2007) 1878–1881.
- [20] G.L. Xiao, S. Li, H. Li, L.Q. Chen, *Microporous Mesoporous Mater.* 120 (2009) 426–431.
- [21] S.Y. Wang, N. Li, R.M. Zhou, L.Y. Jin, G.S. Hu, J.Q. Lu, M.F. Luo, *J. Mol. Catal. A* 374–375 (2013) 53–58.
- [22] D.A. Andersson, S.I. Simak, N.V. Skorodumova, I.A. Abrikosov, B. Johansson, *Phys. Rev. B* 76 (2007) 174119.
- [23] P. Singh, M.S. Hegde, *J. Solid State Chem.* 181 (2008) 3248–3256.
- [24] Y.N. Sun, Z.H. Qin, M. Lewandowski, E. Carrasco, M. Sterrer, S. Shaikhutdinov, H.J. Freund, *J. Catal.* 266 (2009) 359–368.
- [25] G. Samjeske, K.-i. Komatsu, M. Osawa, *J. Phys. Chem. C* 113 (2009) 10222–10228.
- [26] M.F. Camellone, S. Fabris, *J. Am. Chem. Soc.* 131 (2009) 10473–10483.
- [27] Y. Liu, C. Wen, Y. Guo, G.Z. Lu, Y.Q. Wang, *J. Mol. Catal. A* 316 (2010) 59–64.
- [28] A.A. Herzing, C.J. Kiely, A.F. Carley, P. Landon, G.J. Hutchings, *Science* 321 (2008) 1331–1335.
- [29] N. Kamiuchi, M. Haneda, M. Ozawa, *Catal. Today* 201 (2013) 79–84.
- [30] D.R. Schryer, B.T. Upchurch, B.D. Sidney, K.G. Brown, G.B. Hoflund, R.K. Herz, *J. Catal.* 130 (1991) 314–317.
- [31] S.-H. Oh, G.B. Hoflund, *J. Phys. Chem. A* 110 (2006) 7609–7613.
- [32] H.Q. Zhu, Z.F. Qin, W.J. Shan, W.J. Shen, J.G. Wang, *J. Catal.* 233 (2005) 41–50.
- [33] J. Lin, Y. Huang, L. Li, A. Wang, W. Zhang, X. Wang, T. Zhang, *Catal. Today* 180 (2012) 155–160.
- [34] P. Ciambelli, S. Cimino, L. Lisi, M. Faticanti, G. Minelli, I. Pettiti, P. Porta, *Appl. Catal. B* 33 (2001) 193–203.
- [35] S. Cimino, S. Colonna, S. De Rossi, M. Faticanti, L. Lisi, I. Pettiti, P. Porta, *J. Catal.* 205 (2002) 309–317.
- [36] G. Groppi, C. Cristiani, P. Forzatti, *Appl. Catal. B* 35 (2001) 137–148.
- [37] E. Aneggi, C. de Leitenburg, G. Dolcetti, A. Trovarelli, *Catal. Today* 114 (2006) 40–47.
- [38] H.Z. Bao, X. Chen, J. Fang, Z.Q. Jiang, W.X. Huang, *Catal. Lett.* 125 (2008) 160–167.
- [39] J.Y. Luo, M. Meng, X. Li, X.G. Li, Y.Q. Zha, T.D. Hu, Y.N. Xie, J. Zhang, *J. Catal.* 254 (2008) 310–324.
- [40] C.R. Jung, J. Han, S.W. Nam, T.H. Lim, S.A. Hong, H.I. Lee, *Catal. Today* 93–95 (2004) 183–190.
- [41] J.Y. Luo, M. Meng, J.S. Yao, X.G. Li, Y.Q. Zha, X.T. Wang, T.Y. Zhang, *Appl. Catal. B* 87 (2009) 92–103.
- [42] L. Meng, A.P. Jia, J.Q. Lu, L.F. Luo, W.X. Huang, M.F. Luo, *J. Phys. Chem. C* 115 (2011) 19789–19796.
- [43] C.J.G. Van Der Grift, A.F.H. Wielers, B.P.J. Jogh, J. Van Beunum, M. De Boer, M. Versluis-Helder, J.W. Geus, *J. Catal.* 131 (1991) 178–189.
- [44] V.G. Keramidas, W.B. White, *J. Chem. Phys.* 59 (1973) 1561–1562.
- [45] W.H. Weber, K.C. Hass, J.R. McBride, *Phys. Rev. B* 48 (1993) 178–185.
- [46] A. Nakajima, A. Yoshihara, M. Ishigame, *Phys. Rev. B* 50 (1994) 13297–13307.
- [47] Z.Y. Pu, J.Q. Lu, M.F. Luo, Y.L. Xie, *J. Phys. Chem. C* 111 (2007) 18695–18702.
- [48] Y. Li, B.C. Zhang, X.L. Tang, Y.D. Xu, W.J. Shen, *Catal. Commun.* 7 (2006) 380–386.
- [49] M.F. Luo, Y.J. Zhong, X.X. Yuan, X.M. Zheng, *Appl. Catal. A* 162 (1997) 121–131.
- [50] G. Picasso, M. Gutiérrez, M.P. Pina, J. Herguido, *Chem. Eng. J.* 126 (2007) 119–130.
- [51] F.J. Perez-Alonso, I. Melián-Cabrera, M. López Granados, F. Kapteijn, J.L.G. Fierro, *J. Catal.* 239 (2006) 340–346.
- [52] X.L. Tang, B.C. Zhang, Y. Li, Y.D. Xu, Q. Xin, W.J. Shen, *Catal. Today* 93–95 (2004) 191–198.
- [53] C. Li, Y. Sakata, T. Arai, K. Domen, K.-I. Maruya, T. Onishi, *J. Chem. Soc., Faraday Trans. 1* 85 (1989) 929–943.
- [54] A. Martínez-Arias, M. Fernández-García, O. Gálvez, J.M. Coronado, J.A. Anderson, J.C. Conesa, J. Soria, G. Munuera, *J. Catal.* 195 (2000) 207–216.
- [55] O. Dularent, X. Courtois, V. Perrichon, D. Bianchi, *J. Phys. Chem. B* 104 (2000) 6001–6011.
- [56] K. Hadjiiivanov, H. Knözinger, M. Miaylov, *J. Phys. Chem. B* 106 (2002) 2618–2624.
- [57] M.C. Campa, S. De Rossi, G. Ferraris, V. Indovina, *Appl. Catal. B* 8 (1996) 315–331.
- [58] X. Wang, H.Y. Chen, W.M.H. Sachtler, *J. Catal.* 197 (2001) 281–291.
- [59] J. Couple, D. Bianchi, *Appl. Catal. A* 409–410 (2011) 28–38.
- [60] J.B. Benziger, L.R. Larson, *J. Catal.* 77 (1982) 550–553.
- [61] C. Lemire, R. Meyer, V.E. Henrich, S. Shaikhutdinov, H.J. Freund, *Surf. Sci.* 572 (2004) 103–114.
- [62] C. Li, K. Domen, K.-I. Maruya, T. Onishi, *J. Catal.* 123 (1990) 436–442.
- [63] G. Sedmak, S. Hočevá, J. Levec, *J. Catal.* 222 (2004) 87–99.
- [64] D. Teschner, A. Woitsch, O. Pozdnjakova-Tellinger, J. Kröhnert, E.M. Vass, M. Hävecker, S. Zafeiratos, P. Schnörch, P.C. Jentoft, A. Knop-Gericke, R. Schlögl, *J. Catal.* 249 (2007) 318–327.
- [65] M. Guo, J.Q. Lu, Q.Y. Bi, M.F. Luo, *ChemPhysChem* 11 (2010) 1693–1699.
- [66] P. Gawade, B. Bayram, A.-M.C. Alexander, U.S. Ozkan, *Appl. Catal. B* 128 (2012) 21–30.
- [67] D.G. Blackmond, E.I. Ko, *J. Catal.* 94 (1985) 343–352.
- [68] A.P. Jia, G.S. Hu, L. Meng, Y.L. Xie, J.Q. Lu, M.F. Luo, *J. Catal.* 289 (2012) 199–209.